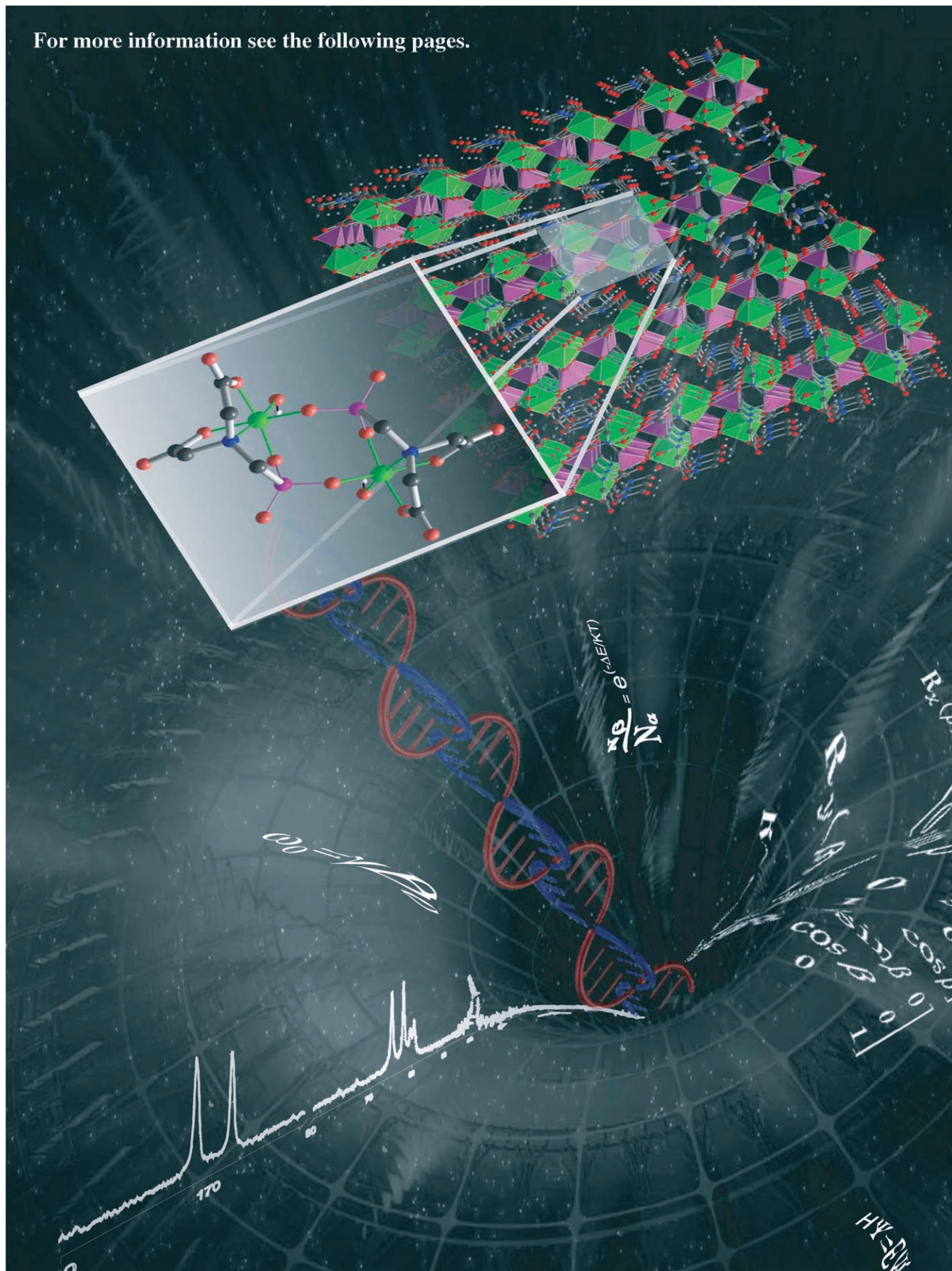For more information see the following pages.

X-ray Diffraction and Solid-State NMR Studies of a Germanium Binuclear Complex

Luís Mafra,[a, b] Filipe A. Almeida Paz,[a] Fa-Nian Shi,[a, c] João Rocha,*[a] Tito Trindade,[a] Christian Fernandez,[b] Anna Makal,[d] Krzysztof Wozniak,[d] and Jacek Klinowski[e]

Abstract: A compound formulated as $(C_4H_{12}N_2)[Ge_2(pmida)_2(OH)_2]\cdot 4H_2O$ (where $pmida^{4-} = N$-(phosphonomethyl)iminodiacetate and $C_4H_{12}N_2^{2+} = $ piperazinedium cation), containing the anionic $[Ge_2(pmida)_2(OH)_2]^{2-}$ complex, has been synthesised by the hydrothermal approach and its structure determined by single-crystal X-ray diffraction analysis. Several high-resolution solid-state magic-angle spinning (MAS) NMR techniques, in particular two-dimensional $^1H-X(^{13}C,^{31}P)$ heteronuclear correlation (HETCOR) and $^1H-^1H$ homonuclear correlation (HOMCOR) experiments incorporating a frequency-switched Lee–Goldburg (FS-LG) decoupling scheme, have been employed for the first time in such a material. Using these tools in tandem affords an excellent general approach to study the structure of other inorganic–organic hybrids. We assigned the NMR resonances with the help of $C\cdots H$ and $P\cdots H$ internuclear distances obtained through systematic statistical analyses of the crystallographic data. The compound was further characterised by powder X-ray diffraction techniques, IR and Raman spectroscopy, and by elemental and thermal analyses (thermogravimetric analysis and differential scanning calorimetry).

Keywords: coordination modes · germanium · hydrothermal synthesis · NMR spectroscopy · organic–inorganic hybrid composites

Introduction

Many inorganic–organic hybrid crystalline materials have been reported to date. Most investigators have used relatively routine (particularly ^1H) NMR techniques to characterise the structures of such solids. This is principally true for materials exhibiting relatively strong bonds between the inorganic and organic components, such as coordination polymers, and contrasts with the important chemical information on organic and inorganic materials generated by high-resolution NMR techniques. We thus aim at assessing the use of multinuclear solid-state magic-angle spinning (MAS) NMR spectroscopy to study inorganic–organic hybrid materials. Although we have begun our studies with crystalline model compounds with relatively simple structures, in the near future we will extend this to coordination polymers and amorphous or disordered inorganic–organic hybrids.

[a] L. Mafra, Dr. F. A. Almeida Paz, Dr. F.-N. Shi, Prof. J. Rocha, Dr. T. Trindade
Department of Chemistry
University of Aveiro, CICECO
3810–193 Aveiro (Portugal)
Fax: (+351) 234-370-084
E-mail: rocha@dq.ua.pt

[b] L. Mafra, Prof. C. Fernandez
Laboratoire Catalyse et Spectrochimie (CNRS UMR 6506)
ENSICAEN and Université de Caen-Basse Normandie
14050 Caen (France)

[c] Dr. F.-N. Shi
College of Chemistry and Environment Science
Nanjing Normal University
210097 Nanjing (P. R. China)

[d] A. Makal, Prof. K. Wozniak
Department of Chemistry, University of Warsaw
Pasteura 1, 02–093 Warszawa (Poland)

[e] Prof. J. Klinowski
Department of Chemistry, University of Cambridge, Lensfield Road, Cambridge CB2 1EW (UK)

N-(phosphonomethyl)iminodiacetic acid (H$_4$pmida, Scheme 1) was previously used in the synthesis of some interesting and useful materials.[1–3] In particular, Clearfield and co-workers[3] prepared a series of layered materials by
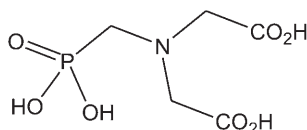
Scheme 1. *N*-(phosphonomethyl)iminodiacetic acid (H$_4$pmida).

partially deprotonating H$_4$pmida, leaving a carboxylic acid group which, on the one hand, allows intercalation of amines and, on the other, forms three-dimensional compounds with diamines. Mixed derivatives containing HPO$_4^{2-}$ moieties which led to the isolation of a family of mixed-ligand layers were also reported by the same authors.[3] More recently, we have isolated the first three-dimensional mixed-metal frameworks incorporating H$_4$pmida residues and 4,4′-bipyridine.[4]

The model hybrid compound studied here is (C$_4$H$_{12}$N$_2$)[Ge$_2$(pmida)$_2$(OH)$_2$]·4H$_2$O, where pmida^{4-} is *N*-(phosphonomethyl)iminodiacetate, which contains the anionic unit Ge$_2$(pmida)$_2$(OH)$_2^{2-}$, closely related to the [V$_2$O$_2$(pmida)$_2$]$^{4-}$ unit. The former, is a particularly convenient unit because it is amenable to NMR studies as it contains no paramagnetic centres (such as V^{4+}) and has the spectroscopically useful nuclei ^{1}H, ^{13}C, and ^{31}P available. As with many hybrid compounds, the solid studied here contains protons in the organic and inorganic components and, thus, the attribution of the ^{1}H NMR resonances is not trivial and requires high-resolution spectra. For this purpose, we have used an FS-LG homonuclear decoupling pulse sequence, inserted in the two-dimensional heteronuclear correlation (HETCOR) and homonuclear correlation (HOMCOR) experiments. Indeed, conventional solid-state NMR techniques, such as MAS and Cross-Polarisation (CP) MAS afford poorly resolved spectra, mainly due to the presence of strong ^{1}H–^{1}H dipolar interactions which broaden the resonances.[5] Since the pioneering work of Lee and Goldburg[6] and Waugh and co-workers,[7] multipulse homonuclear decoupling has been applied to improve the decoupling performance.[5,7–10] Over the last fifteen years, new homonuclear decoupling pulse sequences have been proposed, particularly the frequency-switched Lee–Goldburg (FS-LG) sequence[11] used here. In general, multipulse sequences fail at high MAS rates due to the interference between the sample spinning and radio frequency (rf) cycles. However, with the recent windowless ^{1}H–^{1}H CRAMPS-MAS techniques (for example, FS-LG-2,[5] PM-LG,[10] DUMBO-1[9]) based on off-resonance rf fields, it is possible to simultaneously manipulate the spin and spatial components of the dipolar Hamiltonian, without decreasing the decoupling efficiency. Sequences like FS-LG-2 have short cycle times and, hence, may be combined successfully with moderately fast MAS (up to 12–15 kHz).[12,13]

Experimental Section

General: Chemicals were readily available from commercial sources and were used as received without further purification. Syntheses were carried out in PTFE-lined stainless-steel reaction vessels (10 mL), under autogenous pressure and static conditions. The final compound proved to be air- and light-stable, and insoluble in water and common organic solvents.

Preparation and structural characterisation of (C$_4$H$_{12}$N$_2$)[Ge$_2$(pmida)$_2$(OH)$_2$]·4H$_2$O (I): A suspension containing *N*-(phosphonomethyl)iminodiacetic acid hydrate (0.590 g, H$_4$pmida, C$_5$H$_{10}$NO$_7$P, 97%, Fluka), amorphous germanium(IV) oxide (0.280 g, GeO$_2$, 99.99+%, Aldrich), and anhydrous piperazine (0.090 g, C$_4$H$_{10}$N$_2$, ≥98%, Merck-Schuchardt) in distilled water (approximately 4 g) was stirred thoroughly for 30 min at ambient temperature. The resulting homogeneous suspension was transferred to the reaction vessel which was placed inside an oven. The temperature was gradually increased to 140°C and, after four days, was again increased to 180°C, where it remained for 24 h. The reaction vessel was allowed to cool slowly to ambient temperature before opening. The resultant colourless solution was carefully transferred to a glass container and allowed to evaporate slowly. After one day, a large quantity of colourless crystals were manually harvested, washed with distilled water, and air-dried for single-crystal X-ray diffraction analysis. An alternative synthesis method is to perform the reaction at a fixed temperature of 100°C over a period of four days, after which a phase-pure microcrystalline compound can be directly obtained from the autoclave.

Based on single-crystal data: elemental analysis calcd (%) for C$_{14}$H$_{34}$Ge$_2$N$_4$O$_{20}$P$_2$ (M$_r$ 785.57): C 21.41, N 7.16, H 4.36; found: C 20.61, N 6.98, H 4.40.

Thermogravimetric analysis (TGA) data (weight losses and increases) and derivative thermogravimetric peaks (DTG; in italics inside the parentheses): in air: 50–140°C −9.6% (*77* and *97°C*); 330–420°C −26.5% (*385* and *401°C*); 420–670°C −10.5% (continuous weight-loss); 670–800°C −11.2% (*690°C*); in nitrogen: 45–123°C −9.4% (*72* and *97°C*); 340–425°C −28.4% (*382* and *407°C*); 425–700°C −6.7% (continuous weight-loss); 620–700°C −3.3% (*630°C*); 700–800°C −8.1% (*730°C*); DSC peaks (endothermic processes): 132, 381, and 393°C.

Selected IR data (Raman in italics inside the parentheses): in) ν(O−H, lattice water) and ν(GeO−H) = 3509 (vs) and 3409 (vs) cm^{-1}, ν$_{asym}$(−NH$_2^+$) = 3314 (vs) cm^{-1}, ν$_{sym}$(−NH$_2^+$) = 3214 (vs) cm^{-1}, ν$_{asym}$(C−H in −CH$_2$−) = 3052 (s) and 3015 (s); ν$_{sym}$(C−H in −CH$_2$−) = 2981 (s) and 2963 (s) (*2988* and *2965*); ν(N$^+$−H) = 2740 (m), 2600 (m), and 2460 (m) (various modes); ν(C=O) = 1724 (vs) (*1727*); ν$_{asym}$(−CO$_2^-$) = 1675 (vs) (*1677*); δ(−NH$_2^+$) = 1611 (m); τ(−CH$_2$) = 1463 (m) (*1465*); δ(−CH$_2$−) = 1429 (m) (*1434*) cm^{-1}; ν$_{sym}$(−CO$_2^-$) = 1352 (vs) (*1351*); δ(O−H···O) = 1333 (s) (*1335*); ν(P=O) = 1310 (m) (*1314*) cm^{-1}; ν(C−O) = 1288 (m) and 1270 (m) (*1286* and *1270*); δ(C−C−N, amines) = 1177 (vs) (*1181*) cm^{-1}; ν(N−C) = 1093 (m) and 1077 (s) (*1092* and *1070*); ν (P−O) = 1046 (vs) (*1044*); γ(O−H···O) = 916 (s) (*919*); ν(P−C) = 782 (vs) (*788*); γ(C=O) = 754 (s) and 747 (s) (*743*); ρ[(C=O)−O] 530 (m) and 596 (m) (*535* and *599*); δ(C−N−C, amines) = 455 (m) cm^{-1}.

Characterisation: Elemental analyses for carbon and hydrogen were performed with a FISONS EA1108 instrument.

FTIR spectra were measured from KBr discs (Aldrich, 99%+, FTIR grade) on a Matson 7000 FTIR spectrometer. FTRaman spectra were measured on a Bruker RFS 100 spectrometer with a Nd:YAG coherent laser (λ = 1064 nm).

TGA was carried out using a Shimadzu TGA-50, at a heating rate of 10°C min^{-1}, under a nitrogen atmosphere or air, and a flow rate of 20 cm^3 min^{-1}. DSC analysis was performed by using a Shimadzu DSC-50, at a heating rate of 10°C min^{-1}, under nitrogen atmosphere at a flow rate of 20 cm^3 min^{-1}.

Powder X-ray diffraction patterns were recorded at room temperature using a Philips X'Pert diffractometer, operating with a monochromatic Cu$_{Kα}$ radiation source at 40 kV and 50 mA. Simulated powder patterns were based on single-crystal data, and calculated using the STOE Win XPOW software package.[14]

X-ray crystallography studies: A suitable single-crystal was mounted on a glass fibre with Araldite Rapide,[15] and positioned at approximately 62.25 mm from a KM4CCD/Sapphire charge-coupled device (CCD) area detector. Data were collected at 293(2) K on a KUMA4CCD diffractometer with $Mo_{K\alpha}$ graphite-monochromated radiation ($\lambda = 0.7107$ Å), in the ω scan mode, and controlled by the CrysAlis CCD software package.[16] We measured 600 frames at 1.0° intervals with a counting time of 15 s per frame. We monitored two further standard frames for each 150 frames collected and these showed no significant intensity decrease over the data collection period. Data were corrected for the Lorentz and polarisation effects, and were reduced by using the CrysAlis RED software routines.[17] The structure was solved by the direct methods of SHELXS-97,[18] and refined by full-matrix least-squares on F^2 using SHELXL-97.[19]

All non-hydrogen atoms were directly located from difference Fourier maps and refined with anisotropic displacement parameters. Hydrogen atoms bound to the nitrogen atom of the crystallographically unique piperazinedium cation were directly located from difference Fourier maps, and refined with a common N−H length restrained to 0.90(1) Å (the H···H distance was further restrained to 1.47(1) Å to ensure a chemically reasonable geometry for this moiety), and an isotropic displacement parameter fixed at 1.5 times U_{eq} of the nitrogen atom to which they are attached. Hydrogen atoms from water molecules were directly located from successive difference Fourier maps, and refined with the O−H length and H···H distance restrained to 0.86(1) Å and 1.40(1) Å, respectively (to ensure a chemically reasonable geometry for these molecules), and using a riding model with an isotropic displacement parameter fixed at 1.5 times U_{eq} of the atom to which they are attached. The hydrogen atom associated with the coordinated −OH group to Ge(1) could also be directly located from successive difference Fourier maps, but instead its position was geometrically restrained by using the HFIX 83 instruction in SHELXL.[19] Hydrogen atoms attached to carbon were located at their idealised positions by using the HFIX 23 instruction in SHELXL,[19] and were included the refinement in the riding-motion approximation with an isotropic thermal displacement parameter fixed at 1.2 times U_{eq} of the carbon atom to which they are attached. It is important to emphasise that the positions for the hydrogen atoms do not reflect the true position of the hydrogen nuclei. The last difference Fourier map synthesis showed the highest peak (0.490 e Å⁻³) located at 1.37 Å from O(7), and the deepest hole (−0.455 e Å⁻³) at 0.82 Å from Ge(1).

Information concerning crystallographic data collection and structure refinement details are summarised in Table 1. Selected bond lengths and angles for the binuclear anionic $[Ge_2(pmida)_2(OH)_2]^{2-}$ complex are given in Table 3. Hydrogen bonding geometry is described in Table 4.

CCDC-249364 contains the supplementary crystallographic data (excluding structure factors) for this paper. These data can be obtained free of charge from the Cambridge Crystallographic Data Centre via www.ccdc.cam.ac.uk/data_request/cif.

NMR spectroscopy: Solid-state MAS NMR measurements were performed at 9.4 T on a Bruker Avance 400 spectrometer operating at Larmor frequencies of 400.11, 100.62, and 161.97 MHz for ¹H, ¹³C, and ³¹P nuclei, respectively. Additional ¹³C data was recorded at 11.4 T on a Bruker Ultrashield 500 Avance spectrometer operating at a ¹H Larmor frequency of 500.13 MHz. A 4-mm double-resonance CP/MAS probe was used for the one-dimensional (1D) experiments. The sample was restricted to the middle of a 4-mm ZrO_2 rotor with the help of two plastic inserts (upper and lower insert) in two-dimensional (2D) ¹H{FS-LG}–³¹P HETCOR experiments. Such a procedure is necessary because the FS-LG decoupling step is sensitive to rf inhomogeneities, and leads to an improvement of the rf field homogeneity over the whole volume of the sample. 2D ¹H{FS-LG}–¹H HOMCOR and ¹H{FS-LG}–¹³C HETCOR were performed on a nonrestricted 4-mm rotor.

Efficient heteronuclear decoupling between ¹³C/³¹P and ¹H nuclei was achieved by using the two-pulse phase-modulated (TPPM)[20] decoupling scheme during ¹³C and ³¹P spectral acquisition, with pulse lengths of 4.2 μs (approximately 165° pulses), a phase modulation angle of 15°, and a ¹H rf field strength of $\omega_1/2p$ (nutation frequency) = 100 kHz.

Ramped-amplitude cross-polarisation (RAMP-CP)[21] was used to transfer magnetisation from ¹H to ¹³C/³¹P. RAMP-CP improves the Hart-

Table 1. Crystal data and structure refinement information.

formula	$C_{14}H_{34}Ge_2N_4O_{20}P_2$
formula weight	785.57
crystal system	monoclinic
space group	$C2/c$
a [Å]	12.417(3)
b [Å]	10.091(2)
c [Å]	21.160(4)
β [°]	90.93(3)
volume [Å]	2651.0(10)
Z	4
ρ_{calcd} [g cm⁻³]	1.968
$\mu(Mo_{K\alpha})$ [mm⁻¹]	2.488
F(000)	1600
crystal size [mm]	$0.26 \times 0.21 \times 0.21$
crystal type	colourless prisms
θ range	3.78 to 26.02
index ranges	$-15 \leq h \leq 15$
	$-12 \leq k \leq 12$
	$-25 \leq l \leq 26$
reflections collected	12072
independent reflections	2603 ($R_{int} = 0.0360$)
final R indices [$I > 2\sigma(I)$]	$R_1 = 0.0271$
	$wR_2 = 0.0678$
final R indices (all data)	$R_1 = 0.0323$
	$wR_2 = 0.0699$
largest diff. peak and hole [e Å⁻³]	0.490 and −0.455

mann–Hahn matching condition and the efficiency of the CP step which are known to be very sensitive to rf power instabilities at high MAS rates. With this technique the CP matching profile is less dependent on the MAS rate and thus more easily adjustable and maintainable at optimum Hartmann–Hahn matching for magnetisation transfer. Spectra were referenced against TMS or H_3PO_4 (85 %) at 0 ppm for ¹H, ¹³C, or ³¹P, respectively.

¹H MAS NMR spectroscopy: ¹H MAS NMR spectra were collected with a spinning rate of 30 kHz using a 90° pulse-length of 1.6 μs and a 2 s recycle delay.

¹³C and ³¹P CP/MAS NMR spectroscopy: A RAMP-CP step with a spinning rate of 12 kHz and 15 kHz for ¹³C and ³¹P respectively, was employed with standard phase cycling with a 90° pulse length of 3 μs for ¹H. Contact times were varied between 50 μs and 2 ms. Recycle delays employed were of 5 s and 6 s for ¹³C and ³¹P, respectively. A ¹³C{¹H} RAMP-CP spectrum was also recorded at a static magnetic field of 500 MHz using a 90° pulse length of 3.75 μs and a ¹H nutation frequency ($\omega_1/2\pi$) of 66 kHz.

2D ¹H–X(³¹P,¹³C) HETCOR and 2D ¹H{FS-LG}–¹H HOMCOR experiments were performed by using the pulse sequence (and phase cycling scheme) described in Figure 1a and 1b, respectively. The former pulse scheme was adapted from the sequence described by van Rossum and co-workers.[13] Quadrature detection in t_1 was achieved by using the States-TPPI method.[22] In theory, under FS-LG decoupling, the proton chemical shift is scaled by $1/\sqrt{3}$ (0.57). For the FS-LG HOMCOR/HETCOR schemes, the ¹H chemical shift scale and the scaling factors λ were determined by comparing the 1D ¹H spectra recorded under fast MAS (30 kHz) and under the FS-LG homonuclear decoupling sequence determined by direct comparison with the scaled ¹H{FS-LG}–¹H HOMCOR spectra (See Supporting Information, Figure S1).[23] Scaling factors within the 0.56–0.58 range were obtained for all spectra, which is well within the range of the theoretical value. Experimental parameters are summarised in Table 2.

During τ_{LG} (LG period) the homonuclear proton dipolar coupling is averaged to zero (in a first-order approximation) by applying a rf pulse which initially places the effective field (B_{eff}) at the magic-angle with respect to the static field (B_0).[6] Here ΔLG with phase $+x$ refers to an rf pulse,
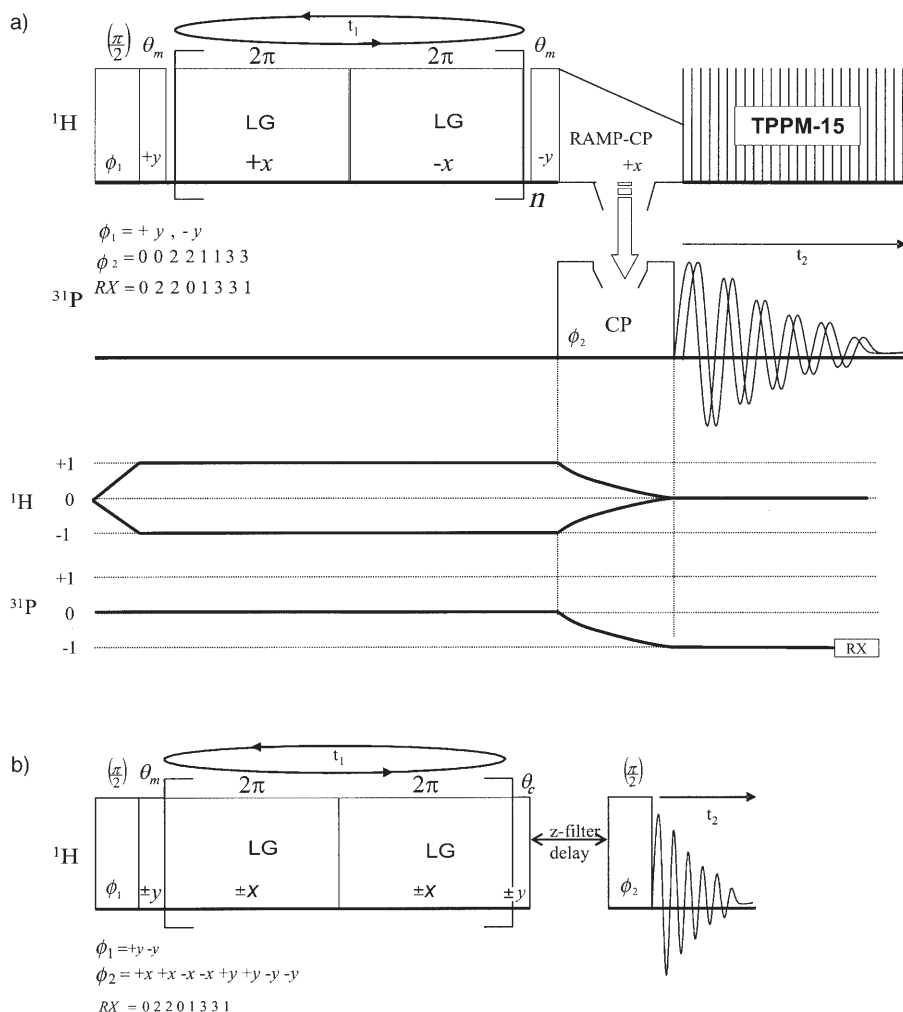
Figure 1. Pulse sequences used to perform 2D: a) ^{1}H{FS-LG}–^{31}P HETCOR with RAMP-CP experiments; b) ^{1}H{FS-LG}–^{1}H HOMCOR. The pulse angle θ_m represents the angle between the static magnetic field (B_0) and the effective field (B_{eff}) direction of the homonuclear sequence used, and denotes the magic-angle. θ_c is the complementary angle, $\theta_c = \pi/2 - \theta_m$.

The pulse sequences employed in these studies (Figure 1) start with a ($\pi/2 + \theta_m$)$_y$ pulse on the proton channel, immediately followed by a train of frequency- and phase-switched symmetric LG pulses in the xz plane. After the evolution period, whereas for HETCOR, proton magnetisation is transferred to the xy plane (detecting plane) followed by TPPM decoupling during acquisition (Figure 1a), for HOMCOR, proton magnetisation is flipped back to the z axis by a single 90°−(θ_m)$_{\pm y}$ pulse (Figure 1b). We have further incorporated a z-filter which ensures that pure absorption-mode line shapes are obtained (Figure 1b).[24]

Results and Discussion

Crystal description: The reaction between H$_4$pmida, germanium(IV) oxide and piperazine in aqueous media led to the formation of a highly crystalline product which was formulated as (C$_4$H$_{12}$N$_2$)[Ge$_2$(pmida)$_2$(OH)$_2$]·4H$_2$O (**I**, where pmida^{4-} = N-(phosphonomethyl)iminodiacetate) on the basis of single-crystal X-ray diffraction (Table 1) and elemental analysis. The phase-purity and homogeneity of the bulk sample were further confirmed by direct comparison of the experimental powder X-ray diffraction pattern and a simulation based on single-crystal data (Figure 2). As predicted, the compound contains an anionic binuclear complex, [Ge$_2$(pmida)$_2$(OH)$_2$]$^{2-}$, sharing similarities with the typical anionic [V$_2$O$_2$(pmida)$_2$]$^{4-}$ units containing V^{4+} centres previously reported (Figure 3).[2,4]

The pmida^{4-} ion appears as a polydentate organic ligand which, in a very similar way to that observed for the V^{4+} centres in [V$_2$O$_2$(pmida)$_2$]$^{4-}$, completely traps the Ge^{4+} inside three distinct five-membered chelate rings formed by the two carboxylate and the phosphonate groups connected in a typical *anti*-unidentate coordinative fashion. The average bite angle is approximately 84.2° (Table 3), a value significantly higher than those registered for the [V$_2$O$_2$(pmida)$_2$]$^{4-}$ units (ap-

with an amplitude ω_{1H} applied to the $+x$ direction with a positive offset of $\Delta\omega$ from the ^{1}H on-resonance frequency fulfilling the condition of $\omega_{1H} = \sqrt{2}\Delta\omega$. For FS-LG, each cycle time consists of two LG blocks. The effective fields created by the two LG units have opposite phases and offset frequencies along the magic-angle.

Table 2. 2D ^{1}H{FS-LG}–^{31}P/^{13}C HETCOR and ^{1}H{FS-LG}–^{1}H HOMCOR experimental parameters for H$_4$pmida and compound **I**.

	^{1}H–^{31}P HETCOR		^{1}H–^{13}C HETCOR		^{1}H–^{1}H HOMCOR
	H$_4$pmida	**I**	H$_4$pmida	**I**	
number of t_1 points	200	200	128	80	172
dwell times ($t_1 \times t_2$) [μs]	8t$_{LG}$×24.8	8t$_{LG}$×24.8	6t$_{LG}$×24.8	6t$_{LG}$×24.8	6t$_{LG}$×12.4
recycle delay [s]	4	4	5	5	3
MAS rate [kHz]	12	12	12	12	10
^{1}H offset frequency [kHz]	+2.5	+2.5	+2.5	+2.5	+4
FS-LG decoupling power [kHz]	100	83.3	83.3	83.3	83.3
contact time [μs]	50–2000	50–2000	50–2000	50–2000	–
FS-LG period −t$_{LG}$ [μs]	9.8	8.2	9.8	9.8	9.8
frequency switching time [μs]	0.6	0.6	0.6	0.6	0.6
positive offset frequency (+ΔLG)[a] [Hz]	73 710	65 925	61 925	61 925	63 925
negative offset frequency (−ΔLG)[a] [Hz]	−67 710	−52 925	−55 925	−55 925	−54 925

[a] These parameters refer to the frequency jumps of $\pm\nu_1/\sqrt{2}$ ($\pm$ΔLG) between each LG period (see Figure 1)
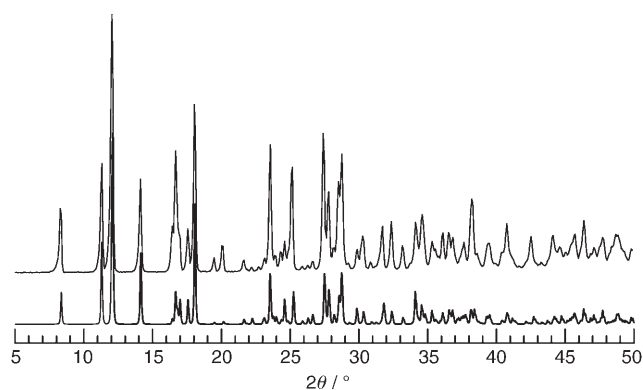
Figure 2. Comparison between the simulated (bottom) and the experimental (top) powder X-ray diffraction patterns.

Table 3. Selected bond lengths [Å] and angles [°] for the binuclear anionic $[Ge_2(pmida)_2(OH)_2]^{2-}$ complex.[a]

Ge(1)−O(1)	1.868(2)	Ge(1)−O(6)	1.897(2)
Ge(1)−O(3)[i]	1.877(2)	Ge(1)−O(8)	1.767(2)
Ge(1)−O(4)	1.930(2)	Ge(1)−N(1)	2.089(2)
O(1)-Ge(1)-O(3)[i]	92.42(7)	O(6)-Ge(1)-O(4)	89.57(8)
O(1)-Ge(1)-O(4)	86.93(8)	O(6)-Ge(1)-N(1)	82.28(7)
O(1)-Ge(1)-O(6)	167.77(7)	O(8)-Ge(1)-O(1)	100.28(8)
O(1)-Ge(1)-N(1)	85.73(7)	O(8)-Ge(1)-O(4)	91.47(8)
O(3)[i]-Ge(1)-O(4)	170.58(7)	O(8)-Ge(1)-O(3)[i]	97.89(8)
O(3)[i]-Ge(1)-O(6)	89.13(8)	O(8)-Ge(1)-O(6)	91.51(8)
O(3)[i]-Ge(1)-N(1)	86.07(7)	O(8)-Ge(1)-N(1)	172.61(8)
O(4)-Ge(1)-N(1)	84.52(7)		

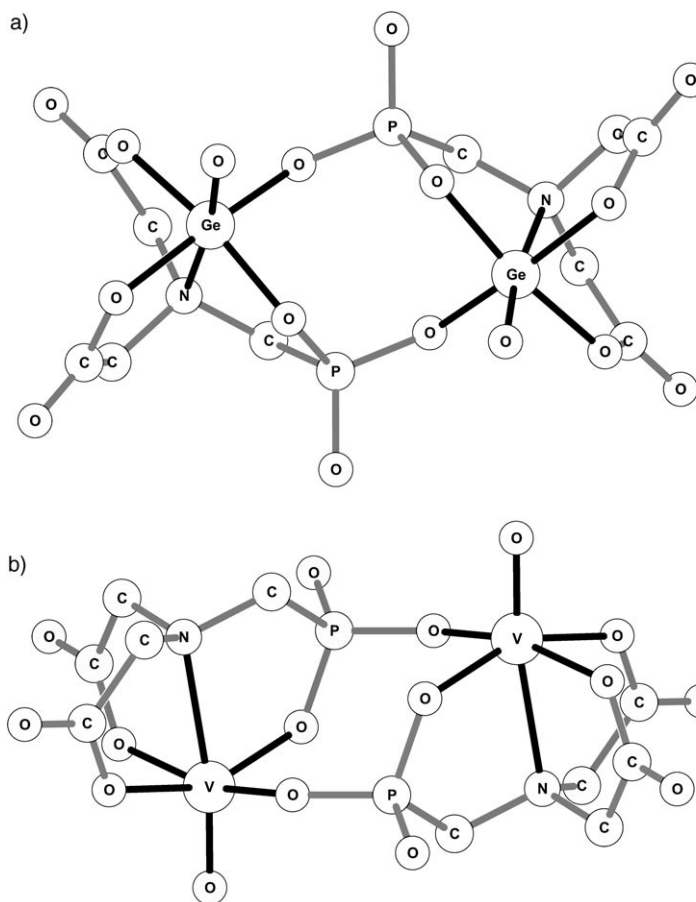[a] Symmetry transformations used to generate equivalent atoms: i: $2-x$, y, $^{1}/_{2}-z$.

a)

b)

Figure 3. Schematic representations of the binuclear anionic: a) $[Ge_2(pmida)_2(OH)_2]^{2-}$; b) $[V_2O_2(pmida)_2]^{4-}$ complexes.

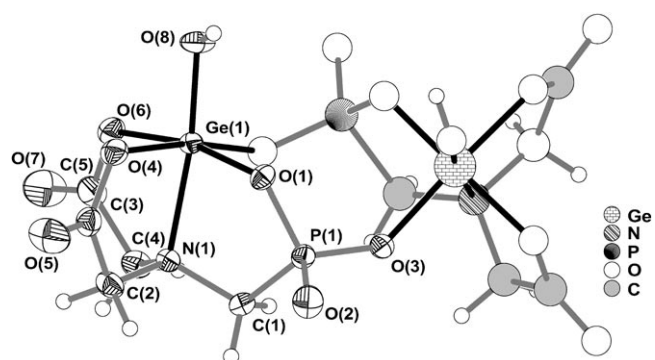Figure 4. Ball-and-stick representation of the binuclear anionic $[Ge_2(pmida)_2(OH)_2]^{2-}$ complex showing the labelling scheme for all non-hydrogen atoms belonging to the asymmetric unit. Displacement ellipsoids are drawn at the 50% probability level and hydrogen atoms are shown as small spheres. For bond lengths and angles see Table 3.

proximateley 76–77°).[2,4] Such an occurrence can be explained by taking the distorted octahedral coordination environment of the single Ge^{4+} centre ($GeNO_5$) into account (octahedral angles within the 82.28(7)–100.28(8)° and 167.77(7)–172.61(8)° ranges; Table 3 and Figure 4). In fact, although the V^{4+} and Ge^{4+} centres in the anionic $[V_2O_2(pmida)_2]^{4-}$ and $[Ge_2(pmida)_2(OH)_2]^{2-}$ complexes, respec-

tively, are almost identically coordinated to two $pmida^{4-}$ ligands, in the former case the apical position is occupied by an oxo ligand (V=O) which has a significant *trans* effect in the V−N length;[25] in **I**, the Ge^{4+} centre is instead coordinated to a hydroxo group (Ge−OH, 1.767(2) Å; Figure 4) having a smaller *trans* effect than the oxo ligand, leading to a Ge−N distance (2.089(2) Å) which is comparable to those observed for the equatorial Ge−O bonds (within the 1.868(2)–1.930(2) Å range). Ultimately, the distance-shift of the Ge^{4+} centre from the equatorial plane, approximately 0.18 Å, is smaller than that usually observed for the V^{4+} metal centre, approximately 0.35–0.39 Å.[2,4] All Ge−O, Ge−OH and Ge−N bond distances are well within the expected ranges found in related compounds.[26]

As previously mentioned, and in a very similar way to that observed in the $[V_2O_2(pmida)_2]^{4-}$ binuclear moieties, the two crystallographically independent carboxylate groups appear both coordinated to the Ge^{4+} centre in a typical *anti*-unidentate coordination fashion but, in this case, the C−O bonds do not remain equivalent upon coordination. In fact there is clear crystallographic evidence for distinct C−O bond lengths for the two carboxylate groups (C(3)−O(4) 1.309(3), C(3)−O(5) 1.214(3), C(5)−O(6) 1.317(3), C(5)−O(7) 1.202(3) Å). Furthermore, the uncoordinated C−O
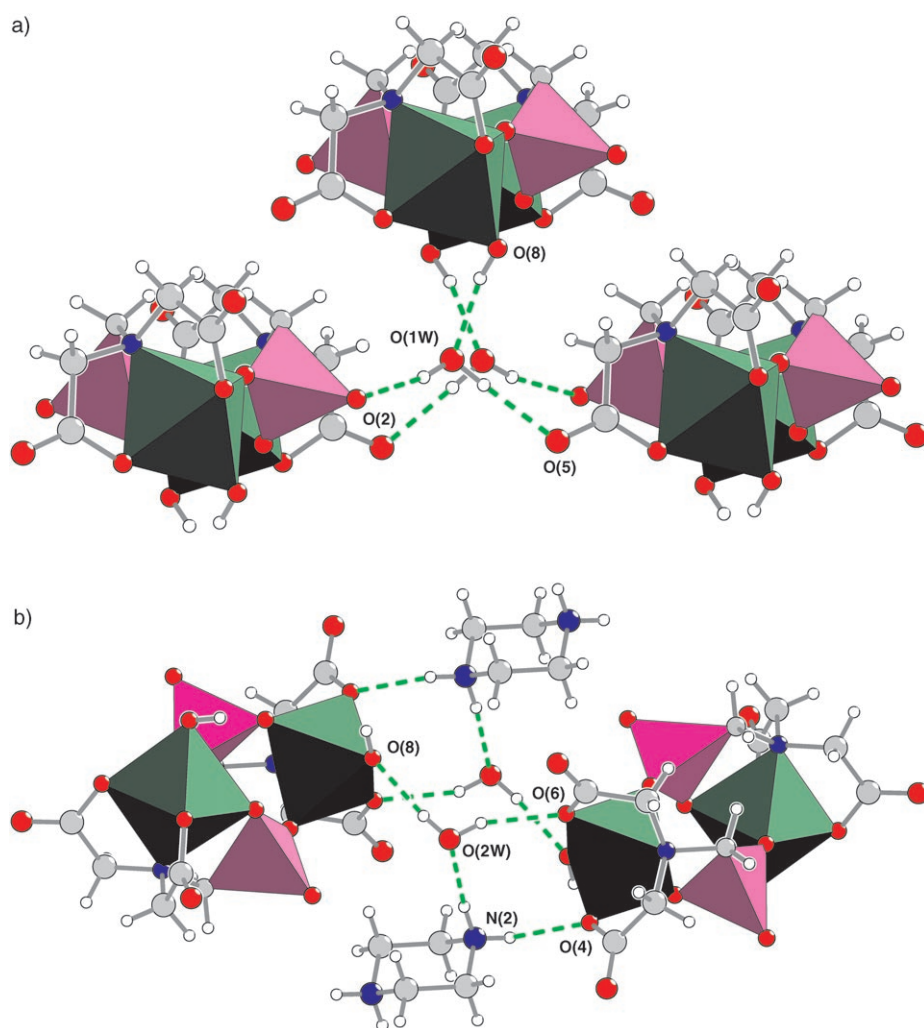
a)

b)

Figure 5. Hydrogen-bonding environment of the crystallisation water molecules: a) O(1W) and b) O(2W) (for hydrogen-bonding geometry see Table 4). Each binuclear anionic [Ge$_2$(pmida)$_2$(OH)$_2$]$^{2-}$ complex is represented by polyhedra for the germanium and phosphorous centres (octahedron and tetrahedron, respectively). Symmetry transformations used to generate equivalent atoms have been omitted for clarity.

bonds are also significantly affected by thermal disorder as seen in Figure 3: for a 50% probability level the elliptical vibration of the oxygen atoms is much larger than that observed for the neighbouring atoms. In fact, although the hydrogen bonding network present in compound **I** involves several very strong and highly directional interactions (see below), these are predominantly orientated towards the coordinated C−O bond. With one uncoordinated C−O bond (belonging to the C(3) carboxylate group) there is a single homonuclear O−H···O interaction, and the C−O bond from the C(5) carboxylate group is not engaged in any type of hydrogen bonding interaction.

As observed for the anionic [V$_2$O$_2$(pmida)$_2$]$^{4-}$ complexes, the phosphonate group from the crystallographically unique pmida^{4-} ligand establishes physical bridges between adjacent germanium centres (through the O(1) and O(3) atoms), ultimately leading to the formation of the binuclear [Ge$_2$(pmida)$_2$(OH)$_2$]$^{2-}$ unit and imposing a Ge(1)···Ge(1)^i separa-

tion of 4.612(2) Å (symmetry code: i: 2−x, y, $^1\!/_2$−z). However, there is a striking crystallographic difference between the two complexes concerning local symmetry: while [V$_2$O$_2$(pmida)$_2$]$^{4-}$ is generated by a centre-of-inversion positioned at its centre of gravity (Figure 3a), [Ge$_2$(pmida)$_2$(OH)$_2$]$^{2-}$ is formed by a two-fold axis operation symmetry (Figure 3b and Figure 4). As a direct consequence, in this complex the two Ge−OH bonds are pointing in the same direction with respect to the plane containing the two neighbouring Ge^{4+} centres (torsion angle of about 68°; Figure 3a and Figure 4). Furthermore, in the [Ge$_2$(pmida)$_2$(OH)$_2$]$^{2-}$ complex the two pmida^{4-} anionic ligands are also closer to each other with an N(1)···N(1)^i separation of 5.574(4) Å (symmetry code: i: 2−x, y, $^1\!/_2$−z) as compared to the smaller values (approximately 5.9 Å) usually observed for the [V$_2$O$_2$(pmida)$_2$]$^{4-}$ moiety.[2,4]

The charge of the anionic complex is compensated by the presence of piperazinedium cations, C$_4$H$_{12}$N$_2$$^{2+}$, which, along with the two water-of-crystallisation molecules, exhibit strong and highly directional hydrogen bonds with the anionic [Ge$_2$(pmida)$_2$(OH)$_2$]$^{2-}$ complexes (Figures 5 and 6, Table 4). On the one hand, each water molecule acts as a bifurcated donor establishing links between adjacent germanium complexes (Figure 5); on the other hand, while O(1W) accepts the hydrogen atom from the coordinated hydroxo group (Figure 5a), O(2W) is involved in a very strong heteronuclear N$^+$−H···O interaction with the neighbouring piperazinedium cation (Figure 5b). It is also interesting to note that the other strong N$^+$−H···O hydrogen bond is with the [Ge$_2$(pmida)$_2$(OH)$_2$]$^{2-}$ complex, leading to the formation of a $R_3^3(8)$ graph set motif (Figure 5b)[27] which further increases the robustness of the crystal structure.

Solid-state MAS NMR spectroscopy: *^{13}C RAMP-CP/MAS NMR*: The ^{13}C{^{1}H} CP/MAS spectra of H$_4$pmida and (C$_4$H$_{12}$N$_2$)[Ge$_2$(pmida)$_2$(OH)$_2$]·4H$_2$O (**I**) are shown in Figure 7. We attributed the peak centred at approximately $\delta = 41$ ppm to the piperazinedium cations. The C(1)−C(5)
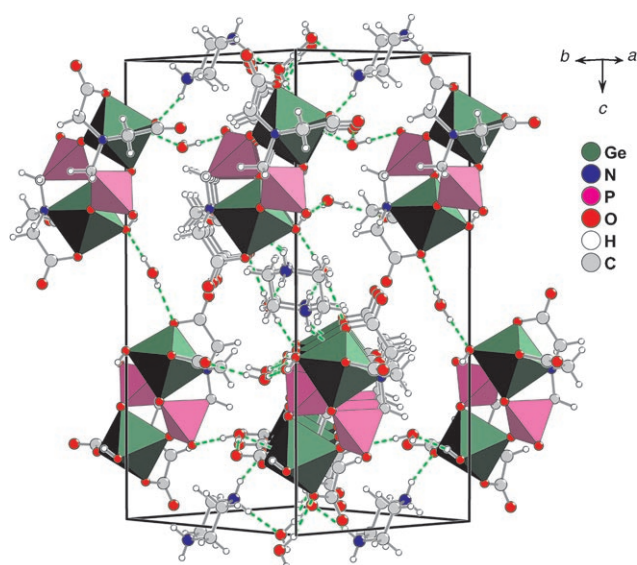
Figure 6. Perspective view of the unit cell contents. Hydrogen bonds are represented as green dashed lines (for hydrogen-bonding geometry see Table 4).

Table 4. Hydrogen-bonding geometry: distances [Å] and angles [°].[a,b]

D−H···A	d(D−H)	d(H···A)	d(D···A)	<(DHA)
O(8)−H(8)···O(1W)^{ii}	0.82	1.88	2.685(3)	164.8
O(1W)−H(1C)···O(2)	0.86(3)	1.83(3)	2.679(3)	169(3)
O(1W)−H(1D)···O(5)^{iii}	0.86(3)	1.96(3)	2.816(3)	177(4)
O(2W)−H(2C)···O(8)^{iv}	0.86(3)	1.89(3)	2.742(3)	173(3)
O(2W)−H(2D)···O(6)^{v}	0.85(3)	2.06(3)	2.872(3)	159(3)
N(2)−H(2E)···O(4)^{vi}	0.87(4)	2.16(4)	2.870(3)	138(3)
N(2)−H(2F)···O(2W)^{vii}	0.87(4)	1.89(4)	2.761(3)	172(4)

[a] The O−H and N−H distances were restrained to 0.86(1) and 0.90(1) Å, respectively. [b] Symmetry transformations used to generate equivalent atoms: ii: $1.5-x$, $-^1/_2+y$, $^1/_2-z$; iii: $1-x$, y, $^1/_2-z$; iv: $x-1$, $1+y$, z; v: $1-x$, $1-y$, $1-z$; vi: x, $1+y$, z; vii: $1-x$, $2-y$, $1-z$.

(Figure 7 and Figure 8): $\delta = 0.7$ and 0.2 ppm for CH_2 groups (C(2), C(4)) and $-CO_2^-$ groups (C(3), C(5)) in the free ligand, and $\delta = 2.9$ and 3.2 ppm for the complex (Figure 7).

Although the crystal structure of compound **I** calls for a single C(1) site, the $^{13}C\{^1H\}$ CP/MAS spectrum displays two resonances (Figure 7b). This splitting (approximately 140 Hz) is attributed to J-coupling interaction, $^1J_{C(1),P(1)}$, an

resonances of compound **I** are shifted to high frequency relative to those of the H$_4$pmida ligand (Figure 7), and this is attributed to the coordination of the H$_4$pmida ligand to the Ge^{4+} centres, which decreases the electron density of the ^{13}C atoms. The combined effect of Ge^{4+} coordination and hydrogen bonding to the piperazinedium cations and water molecules is reflected in the ^{13}C chemical shifts which results in a larger separation of the $-CH_2-CO_2^-$ resonances
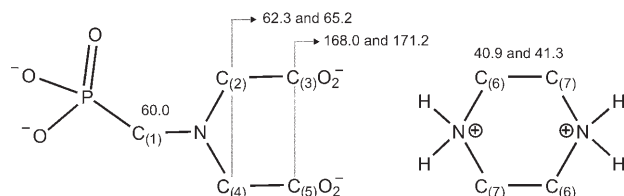

Figure 8. Assignment of the $^{13}C\{^1H\}$ CP/MAS resonances of compound **I**. Chemical shifts are quoted in ppm (spectra in Figure 7b).
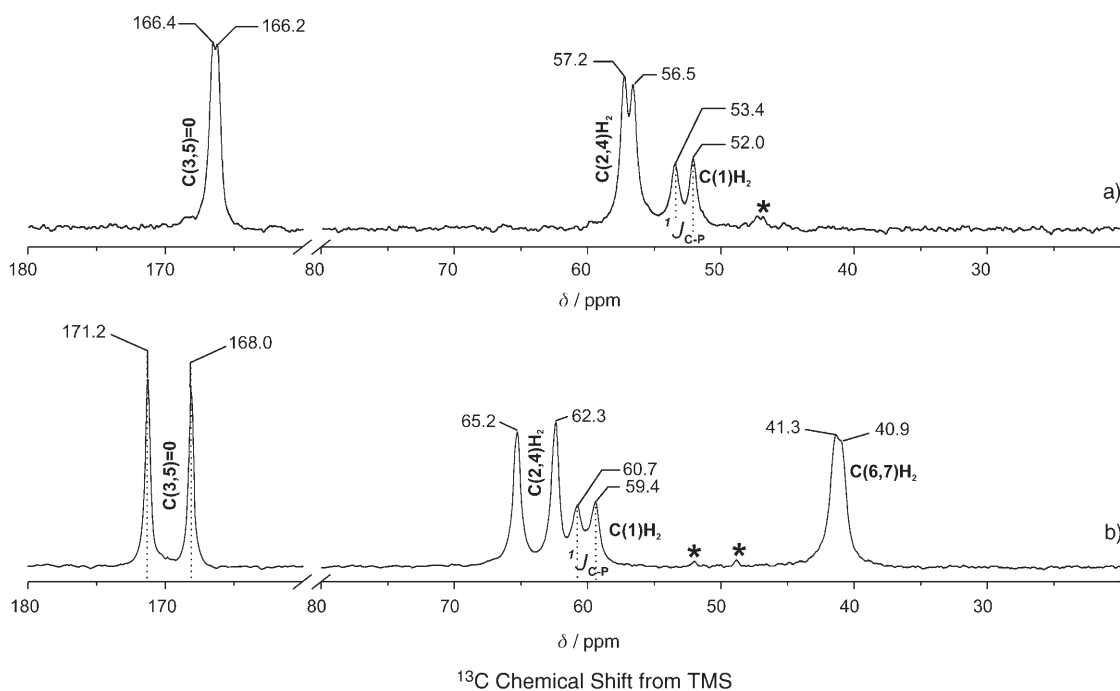

Figure 7. $^{13}C\{^1H\}$ RAMP-CP spectra of: a) H$_4$pmida ligand with a contact time (CT) of 1500 μs; b) compound **I** with a CT of 2000 μs. Asterisks depict the spinning sidebands of the isolated C=O groups.

assumption supported by: 1) the ¹³C NMR spectrum of the free ligand in DMSO (not shown), which shows a splitting of approximately 150 Hz, and 2) the ¹³C{¹H} CP/MAS spectrum recorded at the higher field of 500 MHz (see Supporting Information, Figure S2), which reveals a splitting of about 140 Hz (within experimental error). Typical $^1J_{C,P}$ couplings are in the 5 to 90 Hz range,[28] and spin multiplets are usually not observed in the solid state. A possible reason for observing J-coupling for the H_4pmida ligand and compound **I** is the close proximity of both the electronegative atom N(1) and an electron-withdrawing phosphonate group, leading to a substantial increase of the ^1J coupling magnitude.

³¹P RAMP-CP/MAS NMR: A comparison of the ³¹P{¹H} CP/MAS spectra of H_4pmida and compound **I** shows that upon Ge^{4+} coordination the ³¹P resonance shifts approximately 6 ppm to lower frequency and broadens (full-width-at-half-maximum, FWHM) from 87 (H_4pmida) to 152 Hz (see Supporting Information, Figure S3). We note that the H_4pmida chemical shift measured here ($\delta = 13.1$ ppm) differs from the value $\delta = 14.8$ ppm reported by Khizbullin and co-workers.[29]

Two-dimensional FS-LG experiments: Strong homonuclear dipolar couplings do not usually allow resolution of different resonances using the conventional MAS technique. To improve ¹H spectral resolution we have used FS-LG HOMCOR/HETCOR dipolar correlation techniques. The ¹H{FS-LG}–¹H HOMCOR spectra of H_4pmida and compound **I** display five and three resolved resonances (Fig-
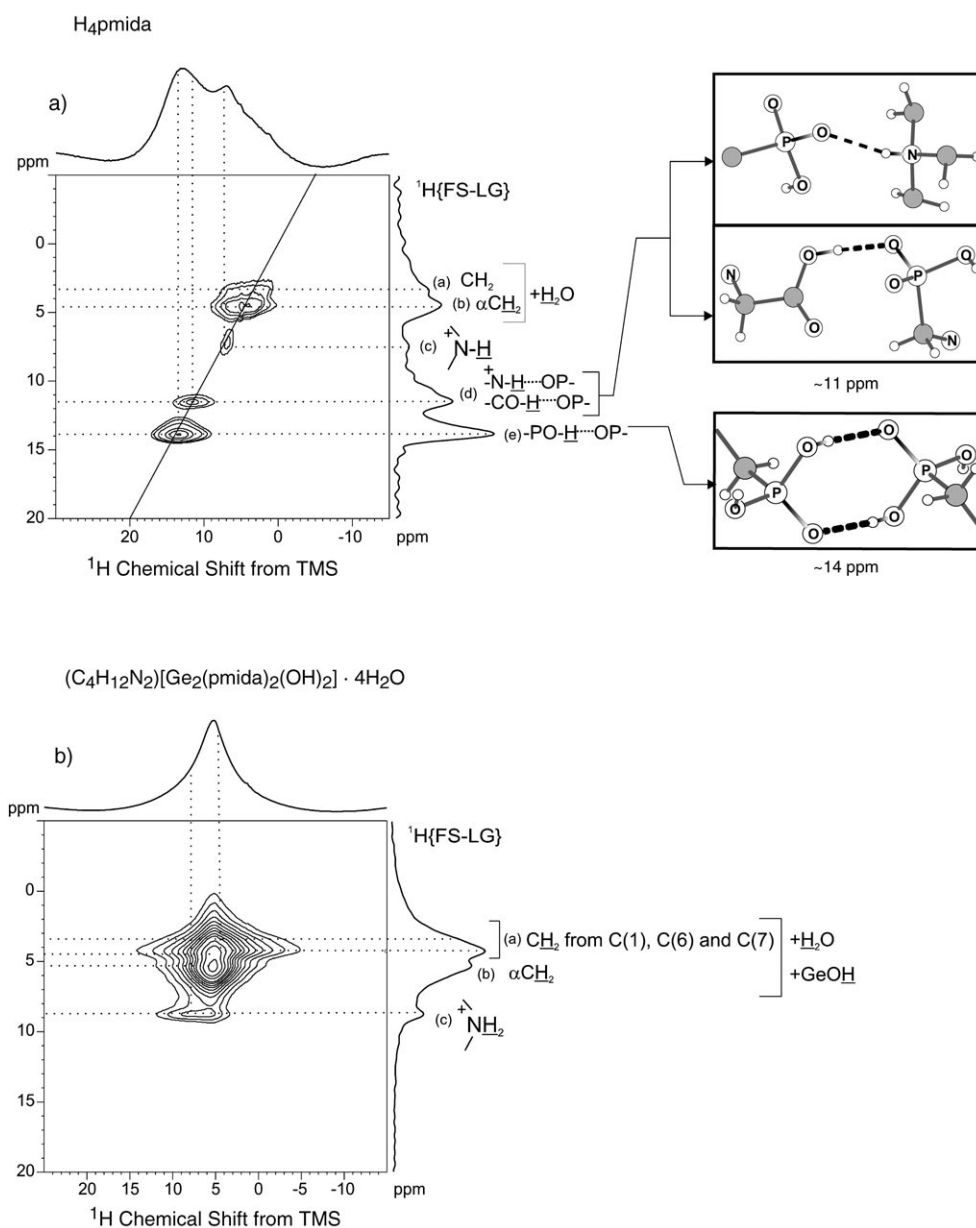
Figure 9. 2D ¹H{FS-LG}–¹H HOMCOR spectra of H_4pmida and compound **I**.

ure 9a,b), respectively. The peak at approximately 8.7 ppm in the spectrum of compound **I** is attributed to the protonated amines of $C_4H_{12}N_2^{2+}$ (Figure 9b).[30]

The 2D ^1H{FS-LG}–^1H HOMCOR spectra of compound **I** and H_4pmida show some similarity in the $\delta = 3.0$–5.5 ppm range (Figure 9), although the intensities of the two resonances (a, b) in this region differ. This is due to the presence of an additional organic molecule in **I** (piperazinedium cations) containing CH_2 groups [$C=C(6,7)$], which also contribute to the intensity of the H(6A), H(6B), H(7A), and H(7B) proton resonances in this spectral region. Because H_4pmida and **I** are hydrated, and the ^1H chemical shift of water molecules is usually in the range $\delta = 4.9$–5.2 ppm, the assignment of ^1H resonances in the CH_2 region becomes even more difficult.

For compound **I** the attribution of the ^+N-H bond resonance was straightforward, whereas this was not the case for H_4pmida, which crystallises in its zwitterionic form, with individual molecular units being involved in several hydrogen-bonding patterns ($P-O-H\cdots O-P$, $C-O-H\cdots O-P$, and $N^+-H\cdots O-P$, with the latter not represented in Figure 9a).[31] Neighbouring molecular units are strongly interconnected by a stable dimer involving two $P-O-H\cdots O-P$ interactions (a typical $R_2^2(8)$ graph set motif).[27] Since hydrogen atoms involved in the $P-O-H\cdots O$ interactions are generally less shielded than those in $C-O-H\cdots O$ or $N^+-H\cdots O$ units, the resonances are shifted to higher frequencies.[32] Hence, the peaks at approximately $\delta = 13.8$ and 11 ppm are assigned to $P-O-H$ and $CO-H/N^+-H$, respectively (Figure 9a). The presence of a resonance at $\delta = 7.5$ ppm (Figure 9a, peak c) supports the assumption that H_4pmida is in the zwitterionic form because it appears in the typical range for protonated amines.

It was difficult to assign the resonances given by the chemically similar CH_2 groups ($\delta = 3.0$–5.5 ppm region) present in compound **I** and H_4pmida. To help solve this problem, we recorded ^1H{FS-LG}–$^{13}C/^{31}P$ HETCOR spectra. By manipulating the mixing time and monitoring the intensity of the cross-peaks in a ^1H{FS-LG}–^{13}C HETCOR experiment it is, in principle, possible to differentiate between ^1H atoms directly bonded (at a short distance) to a given ^{13}C atom from those which are at longer distances. Although FS-LG homonuclear decoupling greatly reduces the spin diffusion, during the CP step the homogeneous broadening (the flip-flop terms) is partially reintroduced, and degrades the spectral resolution.[33] If relaxation effects are neglected, there are two main ways to minimise spin–diffusion effects during the CP step: 1) ^1H magnetisation transfer using Lee–Goldburg cross polarisation (LG-CP);[34] and 2) the more classical approach in which very short mixing times are employed. The latter method (mixing times of 50–200 μs) is used here due to its easy implementation.

At long contact times (2000 μs), cross-peaks are observed between all ^1H and ^{13}C resonances in the H_4pmida spectrum (see Supporting Information, Figure S4). The shoulder at approximately 3.5 ppm F1 (Figure S4, peak a) is assigned to the ^1H atoms bonded to C(1) [H(1A), H(1B)] because they

are more shielded than the αCH_2. By employing a contact time of 100 μs, cross-peaks of ^1H involved in hydrogen bonds disappear. In addition, the cross-peaks with carboxylic ^{13}C (closest protons at approximately 2.5 Å) are also absent. At present, we can not explain why C(1) cross-peaks disappear almost completely. At short contact times it is possible to distinguish the H(2A), H(2B), and the H(4A), H(4B) ^1H resonances, at $\delta \approx 4.8$ and 5.1 ppm, given by the αCH_2 groups. The same is observed in the ^1H{FS-LG}–^{31}P HETCOR spectra (see Supporting Information, Figure S5).

In the $\delta = 3.0$–5.5 ppm region, the F1 projection of the ^1H{FS-LG}–^{13}C HETCOR of **I** (Figure 10) is slightly less resolved than that of the ^1H{FS-LG}–^1H HOMCOR spectrum (Figure 9b), probably due to spin–diffusion occurring during CP. For a contact time of 2000 μs the cross-peaks between C(1) and H(2E) and H(2F) are not very intense. A statistical analysis based on crystallographic data for the C(1–5)$\cdots$H distances within a 5 Å radius, reveals that C(1) is: 1) the farthest ^{13}C nucleus from the neighbouring ^1H (median 4.17 Å, Figure 11), and 2) it only has a single ^1H from a piperazinedium cation within this 5 Å radius sphere (H(2E) at 4.11 Å). This analysis can be further used to assign the C(2)–C(5) resonances. As far as the two carboxylic ^{13}C resonances are concerned, the 171.2 ppm cross-peak is stronger and, thus, the nuclei giving this resonance are likely to be closer to the ^1H reservoir. The box plots (Figure 11) and the C$\cdots$H distances (see Supporting Information, Figure S10) indicate that the C(3) is closer than C(5) to ^1H (median value of 4.05 Å versus 4.10 Å). Furthermore, since C(3) is also closer than C(5) to H(2E) and/or H(2F), with distances 3.21–3.98 Å and 4.22–4.64 Å, respectively, we believe that C(3) gives the resonance at 171.2 ppm (Figure 10). The resonance at 62.3 ppm is tentatively assigned to C(4) because this ^{13}C nucleus is closer than C(2) to H(2E) and H(2F) (see Supporting Information, Figure S11), and also closer to the ^1H reservoir within a 5 Å radius sphere (median 3.91 Å, 75 % of distances < 4.13 Å, Figure 11). Using the same rationale, the peak at 65.2 ppm is attributed to C(4) (median of 3.95 Å and 75 % of distances < 4.47 Å).

The ^1H{FS-LG}–^{13}C HETCOR spectrum of **I** recorded with a contact time of 50 μs (Figure 8), reveals that the αCH_2 protons resonate at $\delta \approx 5.1$ ppm; these are the most acidic protons, expected to be more deshielded than the other CH_2 protons in the structure. Furthermore, spectral analysis shows that the protons of the piperazinedium cations and C(1) are chemically similar, giving overlapping resonances at $\delta \approx 4.5$ ppm (Figure 7). However, there is a noticeable shoulder at $\delta \approx 3.5$ ppm in the ^1H{FS-LG}–^1H HOMCOR (Figure 9B), also observed in the F1 projection of the ^1H{FS-LG}–^{13}C HETCOR spectrum (Figure 10), which contributes to the cross-peak at $\delta \approx 41$ ppm of F2.

The phosphorus atom, P(1), is structurally positioned in what can be considered as the interface between the organic and the inorganic components of **I**. Because there are no protons directly connected to P(1), ^{31}P is a good nucleus to probe the neighbouring ^1H environments. At short contact times (50 μs), the ^1H{FS-LG}–^{31}P HETCOR spectrum of **I**
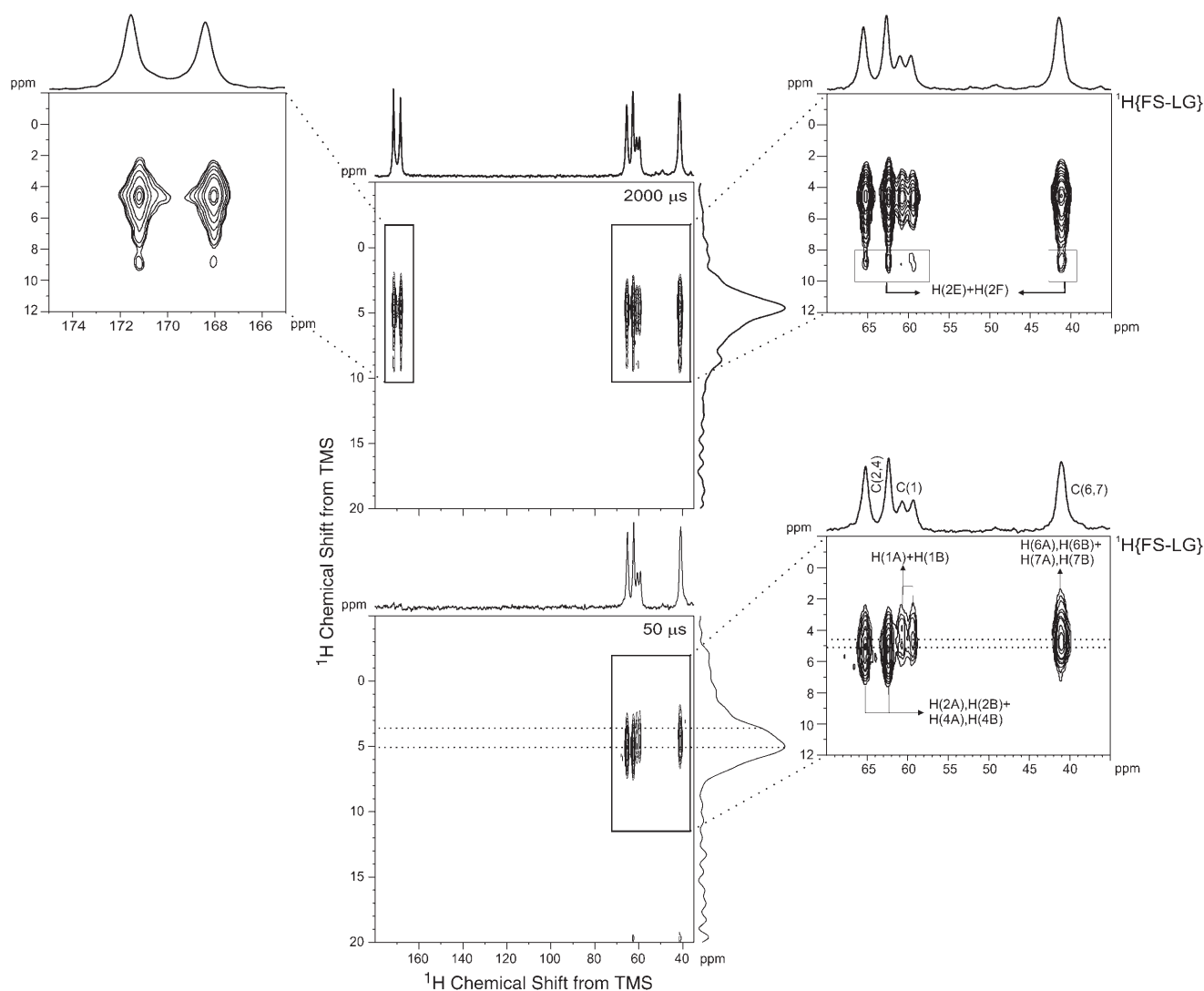
Figure 10. 2D ^{1}H{FS-LG}–^{13}C HETCOR spectra of compound **I** recorded with contact times of 50 and 2000 µs.
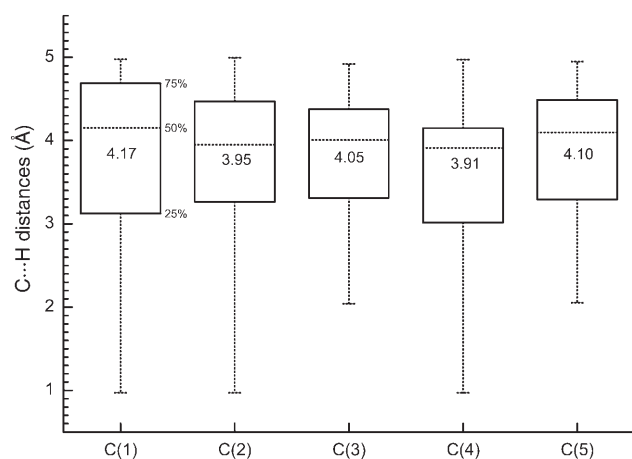

Figure 11. Observed C···H distances (in Å) for C(1)–C(5) represented as box plots giving median (also inside the boxes), upper (75%), and lower (25%) quartiles, and maximum and minimum values. Detailed C···H distances are given in the Supporting Information, Figures S8–S12.

shows the resonance at $\delta \approx 3.5$ ppm resolved from that at $\delta \approx 4.3$ ppm (See Supporting Information, Figure S6). Taking into account the P···H distances (See Supporting Information, Figure S7) and the ^{1}H{FS-LG}–^{13}C HETCOR spectra (Figure 10), the former resonance is assigned to protons from C(7), the latter to those from C(1), C(6), and possibly water, in good agreement with the crystallographic non-equivalence of the piperazinedium ^{13}C atoms. Moreover, for a contact time of 2000 µs the ^{1}H{FS-LG}–^{31}P HETCOR spectrum (see Supporting Information, Figure S6) exhibits two additional resonances at $\delta \approx 5.1$ and 8.7 ppm, attributed to αCH$_2$ and $^+$NH$_2$, respectively (see Supporting Information, Figure S7).

Thermal analysis: Thermal treatment of (C$_4$H$_{12}$N$_2$)[Ge$_2$(pmida)$_2$(OH)$_2$]·4H$_2$O in air and nitrogen result in very similar decomposition processes (see Experimental Section). Below 140°C the compound releases all the water-of-crystallisation molecules with registered weight losses of 9.6% and 9.4%

(for air and nitrogen atmosphere, respectively) which is in good agreement with the theoretical value for the four molecules (9.2%). The "dehydrated" material is then thermally stable up to approximately 330°C, when decomposition starts, involving several consecutive weight losses, strongly indicating a multi-step and complex decomposition. The overlapping decomposition steps led to difficulties in identifying the components that are released at a given temperature. However, between ambient temperature and 800°C a combined weight loss of 42.2% and 44.1% (for air and nitrogen atmosphere, respectively) agrees well with the calculated value of 44.7% for the formation of the stoichiometric amount of $Ge_2O(PO_4)_2$.

Vibrational spectroscopy: FT-IR and FT-Raman spectroscopy confirm the presence of the primary building blocks of $(C_4H_{12}N_2)[Ge_2(pmida)_2(OH)_2] \cdot 4 H_2O$, through the typical vibrations of phosphonate groups and tertiary/secondary amines, and the vibrational modes for carboxylic acid groups. The spectra are also particularly informative concerning the extensive hydrogen-bonding sub-network which involves the water-of-crystallisation molecules ($\nu(O-H)$, δ-$(O-H\cdots O)$ and $\gamma(O-H\cdots O)$ vibrational modes), the carboxylate, $Ge-OH$ and $-NH_2^+$ groups. The measured value of $\Delta[_{asym}(-CO_2^-)-\nu_{sym}(-CO_2^-)]$ gives further structural information concerning the coordination mode of the carboxylate groups:[35] the calculated value of 323 cm^{-1} is typical of the unidentate coordination mode, as revealed by the X-ray diffraction analysis.

Conclusion

We have successfully isolated the binuclear Ge^{4+} complex $[Ge_2(pmida)_2(OH)_2]^{2-}$, closely related to the $[V_2O_2-(pmida)_2]^{4-}$ unit, previously used to construct three-dimensional coordination frameworks through a hydrothermal approach. By replacing the paramagnetic V^{4+} centres by Ge^{4+} we were able to explore the use of high-resolution solid-state NMR techniques to study a model inorganic–organic compound. This is part of a systematic effort to evaluate the potential use of these tools to elucidate the structure inorganic–organic hybrid materials, including those which are amorphous or disordered.

The local ^{13}C and ^{31}P environments of H_4pmida and $(C_4H_{12}N_2)[Ge_2(pmida)_2(OH)_2] \cdot 4 H_2O$ were probed by using the $^{13}C/^{31}P\{^1H\}$ RAMP-CP method, showing that the coordination to the Ge^{4+} centres shifts all pmida^{4-} carbon resonances to high frequency, thus clearly resolving the $-CH_2-CO_2^-$ resonances. The resolution of the ^1H spectra was much improved (relative to "conventional" MAS) by using the frequency-switched Lee–Goldburg (FS-LG) decoupling scheme in HOMCOR/HETCOR dipolar correlation techniques. Comparison between 2D $^1H\{FS-LG\}-^1H$ HOMCOR spectra allowed the systematic study of the hydrogen bonding interactions in H_4pmida and $(C_4H_{12}N_2)[Ge_2(pmida)_2(OH)_2] \cdot 4 H_2O$, particularly in the region above $\delta =$

5 ppm. As the structures contain several CH_2 groups, which give overlapping resonances in the $\delta = 3.0–5.5$ ppm range, 2D $^1H\{FS-LG\}-^{13}C/^{31}P$ HETCOR experiments with variable mixing times were performed. This work, combined with the analysis of the crystallographic $C\cdots H$ and $P\cdots H$ internuclear distances, allowed the assignment of the CH_2 resonances.

Acknowledgements

[1] H. X. Pei, S. M. Lu, Y. X. Ke, J. M. Li, S. B. Qin, S. X. Zhou, X. T. Wu, W. X. Du, *Struct. Chem.* **2004**, *14*, 207; S. O. H. Gutschke, D. J. Price, A. K. Powell, P. T. Wood, *Angew. Chem.* **1999**, *111*, 1158; *Angew. Chem. Int. Ed.* **1999**, *38*, 1088.

[2] D. C. Crans, F. L. Jiang, O. P. Anderson, S. M. Miller, *Inorg. Chem.* **1998**, *37*, 6645.

[3] J. G. Mao, A. Clearfield, *Inorg. Chem.* **2002**, *41*, 2319; J. G. Mao, Z. Wang, A. Clearfield, *Inorg. Chem.* **2002**, *41*, 6106; A. Clearfield, C. V. K. Sharma, B. Zhang, *Chem. Mater.* **2001**, *13*, 3099; B. L. Zhang, D. M. Poojary, A. Clearfield, G. Z. Peng, *Chem. Mater.* **1996**, *8*, 1333.

[4] F. A. A. Paz, F. N. Shi, J. Klinowski, J. Rocha, T. Trindade, *Eur. J. Inorg. Chem.* **2004**, 2759.

[5] A. Bielecki, A. C. Kolbert, M. H. Levitt, *Chem. Phys. Lett.* **1989**, *155*, 341.

[6] M. Lee, W. I. Goldburg, *Phys. Rev.* **1965**, *140*, 1261.

[7] J. S. Waugh, L. M. Huber, U. Haeberlen, *Phys. Rev. Lett.* **1968**, *20*, 180.

[8] W. K. Rhim, D. D. Elleman, R. W. Vaughan, *J. Chem. Phys.* **1973**, *59*, 3740; P. Mansfield, *J. Phys. Chem.* **1971**, *75*, 1444; D. P. Burum, W. K. Rhim, *J. Chem. Phys.* **1979**, *71*, 944; D. P. Burum, M. Linder, R. R. Ernst, *J. Magn. Reson.* **1981**, *44*, 173; K. Takegoshi, C. A. McDowell, *J. Chem. Phys.* **1985**, *82*, 100; M. Hohwy, P. V. Bower, H. J. Jackobsen, N. C. Nielsen, *J. Chem. Phys.* **1997**, *106*, 297; M. Hohwy, N. C. Nielsen, *J. Chem. Phys.* **1997**, *106*, 7571; E. Vinogradov, P. K. Madhu, S. Vega, *Chem. Phys. Lett.* **2000**, *329*, 207; E. Vinogradov, P. K. Madhu, S. Vega, *J. Chem. Phys.* **2001**, *115*, 8983; E. Vinogradov, P. K. Madhu, S. Vega, *Chem. Phys. Lett.* **2002**, *354*, 193.

[9] D. Sakellariou, A. Lesage, P. Hodgkinson, L. Emsley, *Chem. Phys. Lett.* **2000**, *319*, 253.

[10] E. Vinogradov, P. K. Madhu, S. Vega, *Chem. Phys. Lett.* **1999**, *314*, 443.

[11] M. H. Levitt, A. C. Kolbert, A. Bielecki, D. J. Rubben, *Solid State Nucl. Magn. Reson.* **1993**, *2*, 151.

[12] B. J. van Rossum, F. Castellani, K. Rehbein, J. Pauli, H. Oschkinat, *ChemBioChem* **2001**, *2*, 906; B. J. van Rossum, C. P. de Groot, V. Ladizhansky, S. Vega, H. J. M. de Groot, *J. Am. Chem. Soc.* **2000**, *122*, 3465; B. J. van Rossum, E. A. M. Schulten, J. Raap, H. Oschkinat, H. J. M. de Groot, *J. Magn. Reson.* **2002**, *155*, 1.

[13] B. J. van Rossum, H. Forster, H. J. M. de Groot, *J. Magn. Reson.* **1997**, *124*, 516.

[14] STOE, Win XPOW THEO (Version 1.15), STOE & Cie GmbH, **1999**.

[15] T. Kottke, D. Stalke, *J. Appl. Crystallogr.* **1993**, *26*, 615.

[16] KUMA, CRYSALIS CCD, Kuma Diffraction, Wroclaw, Poland, **1999**.

[17] KUMA, CRYSALIS RED, Kuma Diffraction, Wroclaw, Poland, **1999**.

[18] G. M. Sheldrick, SHELXS-97, Program for Crystal Structure Solution, University of Göttingen (Germany) **1997**.

[19] G. M. Sheldrick, SHELXL-97, Program for Crystal Structure Refinement, University of Göttingen (Germany) **1997**.

[20] B. M. Fung, A. K. Khitrin, K. Ermolaev, *J. Magn. Reson.* **2000**, *142*, 97.

[21] G. Metz, X. L. Wu, S. O. Smith, *J. Magn. Reson. Ser. A* **1994**, *110*, 219.

[22] D. J. States, R. A. Haberkorn, D. J. Ruben, *J. Magn. Reson.* **1982**, *48*, 286.

[23] A. Lesage, L. Duma, D. Sakellariou, L. Emsley, *J. Am. Chem. Soc.* **2001**, *123*, 5747.

[24] J. P. Amoureux, C. Fernandez, S. Steuernagel, *J. Magn. Reson. Ser. A* **1996**, *123*, 116.

[25] S. Boudin, A. Guesdon, A. Leclaire, M. M. Borel, *Int. J. Inorg. Mater.* **2000**, *2*, 561.

[26] C. Bibal, S. Mazieres, H. Gornitzka, C. Couret, *Organometallics* **2002**, *21*, 2940; M. D. Chen, J. Zhu, S. Z. Hu, *Main Group Met. Chem.* **1999**, *22*, 105; S. J. Lin, Y. J. Chen, J. H. Chen, F. L. Liao, S. L. Wang, S. S. Wang, *Polyhedron* **1997**, *16*, 2843; H. C. Chiang, S. M. Lin, C. H. Ueng, *Acta Crystallogr. Sect. C* **1992**, *48*, 991; A. B. Ilyukhin, L. M. Shkolnikova, Seifullina, II, T. P. Batalova, N. M. Dyatlova, *Koord. Khim.* **1991**, *17*, 795; T. Mizuta, T. Yoshida, K. Miyoshi, *Inorg. Chim. Acta* **1989**, *165*, 65; C. Glidewell, M. B. Hursthouse, D. Lloyd, K. W. Lumbard, R. L. Short, *J. Chem. Res. Synop.* **1986**, 400; R. R. Holmes, R. O. Day, A. C. Sau, C. A. Poutasse, J. M. Holmes, *Inorg. Chem.* **1985**, *24*, 193.

[27] J. Bernstein, R. E. Davis, L. Shimoni, N. L. Chang, *Angew. Chem.* **1995**, *107*, 1689; *Angew. Chem. Int. Ed. Engl.* **1995**, *34*, 1555.

[28] E. Gacs-Baitz, L. A. Wozniak, M. Kajtar-Peredy, *Chirality* **2000**, *12*, 675; A. Ben Akacha, S. Barkallah, H. Zantour, *Magn. Reson. Chem.* **1999**, *37*, 916.

[29] F. F. Khizbullin, B. P. Strunin, E. I. Maslennikov, Y. B. Yasman, V. D. Simonov, *J. Struct. Chem.* **1986**, *27*, 394.

[30] J. Z. Hu, F. Zhou, F. Deng, F. Hanqiao, N. Yang, L. Li, C. Ye, *Solid State Nucl. Magn. Reson.* **1996**, *6*, 85.

[31] L. M. Shkolnikova, M. A. Poraikoshits, N. M. Dyatlova, G. F. Yaroshenko, M. V. Rudomino, E. K. Kolova, *J. Struct. Chem.* **1982**, *23*, 737.

[32] R. M. Silverstein, F. X. Webster, *Spectroscopic Identification of Organic Compounds*, 6th ed., Wiley, New York, **1998**.

[33] K. J. D. Mackenzie, M. E. Smith, *Multinuclear Solid-State Nuclear Magnetic Resonance of Inorganic Materials*, Pergamon Press Inc., Elsevier Science, **2002**.

[34] J. Brus, A. Jegorov, *J. Phys. Chem. A* **2004**, *108*, 3955; M. Hong, X. L. Yao, K. Jakes, D. Huster, *J. Phys. Chem. B* **2002**, *106*, 7355; V. Ladizhansky, S. Vega, *J. Chem. Phys.* **2000**, *112*, 7158.

[35] C. Oldham, in *Comprehensive Coordination Chemistry, Vol. 2*, 1st ed. (Ed.: G. Wilkinson), Pergamon Press, **1987**, p. 435; G. B. Deacon, R. J. Phillips, *Coord. Chem. Rev.* **1980**, *33*, 227.